

PAPER

Native antimony emplaced by methane-rich hydrothermal fluid in an orogenic fault-zone

Michel Jébrak¹  | Charline Lebrun² | Anne-Sylvie André-Mayer² | Marjorie Simard³

¹Département des Sciences de la Terre et de l'atmosphère, Université du Québec à Montréal, Montréal, QC, Canada

²GeoRessources, Université de Lorraine-CNRS-CREGU, Vandœuvre-lès-Nancy Cedex, France

³Agnico-Eagle, division Lapa, Rivière-Héva, QC, Canada

Correspondence

Michel Jébrak, Département des Sciences de la Terre et de l'atmosphère, Université du Québec à Montréal, Montréal, QC, Canada.
Email: jebrak.michel@uqam.ca

Funding information

Natural Sciences and Engineering Research Council of Canada

Abstract

Antimony-rich gold deposits represent a subclass of orogenic hydrothermal systems. The study of the Lapa gold deposit in the Abitibi greenstone belt shows that antimony occurs during two different stages: (1) as early prograde Sb–Ni disseminated sulphides in talc schists, associated with CO₂-bearing fluids, and (2) as a late native antimony association, associated with methane-bearing fluids indicating a reducing environment. Methane could be related to the serpentinization of the ultramafic rocks of the Piché Group hosting the Lapa deposit. Several deposits display the same methane antimony association along fault zones.

1 | INTRODUCTION

Large tectonic fault zones have been recognized on all the Archaean cratons. They represent the ancient equivalent of modern-day continental shear zones (Kerrick & Ludden, 2000). Numerous mineral deposits are associated with these fault zones, including deposits of gold, copper, zinc and antimony (Goldfarb et al., 2005; Kerrich, 1986). Among these elements, antimony is of special interest as it has been recognized as a strategic metal (European Commission, 2011).

Antimony is frequently associated with gold. These two elements occur in epithermal deposits, where Sb, like Hg, marks the top of the low sulphidation system (Cooke & Simmons, 2000; White & Hedenquist, 1990), as well as in Carlin-type deposits (Xie et al., 2017), marine sediments (Lehrberger, 1992) and black shales (Zhai et al., 2014). The most frequent association is with lode gold deposits that are associated with major brittle–ductile faults in mafic/ultramafic volcanic rocks and sediments (Berger, 1993; Dubé & Gosselin, 2007; Groves, Goldfarb, Gebre-Mariam, Hagemann, & Robert, 1998). Gold and associated elements would have been deposited at the end of, and even after, the last increment of deformation (Colvine, 1989; Goldfarb & Groves, 2015; Groves et al., 1998). In such settings, gold is the product of regional hydrothermal H₂O–CO₂ fluids, inherent to metamorphism along convergent margins (Goldfarb, Groves, & Gardoll, 2001; Phillips & Evans, 2004).

These settings have produced 40% of the world's antimony and have been mined in terranes ranging in age from Archaean, such as the “Antimony Line” in South Africa (Davis, Paterson, & Griffiths, 1986; Jaguin et al., 2013; Pearton & Viljoen, 1986) and the Wiluna deposit in Western Australia (Czarnota, Blewett, & Goscombe, 2010; Hagemann & Lüders, 2003), to Phanerozoic, such as Hilgrove in New South Wales, Australia (Ashley & Craw, 2004; Boyle, 1990), Baogutu in northwest China (An & Zhu, 2010; Zheng, Zhu, An, Huang, & Qiu, 2015), La Lucette in France (Chauris & Marcoux, 1994; Pochon et al., 2016) and the Sarylakk and Sentachan deposits in Sakha-Yakutia, Russia (Bortnikov, Gamunin, Vilent'eva, Prokof'ev, & Prokop'ev, 2010). The deposits are hosted by low-grade, greenschist facies regionally metamorphosed rocks and may include stratabound gold–antimony mineralized rocks. No silver or mercury is produced from these deposits. Stibnite and arsenopyrite were also important contributors to the melt that formed the large Hemlo deposit, Ontario (Tomkins, Pattison, & Zaleski, 2004).

In this article, we focus on the Lapa mine, a gold deposit situated along the Cadillac-Larder Lake Fault Zone (CLLFZ) in the Archaean Abitibi greenstone belt of Canada. Using mineralogical and fluid inclusion studies, we show that Sb concentrations are polyphased and could be related to fluid evolution in relation to the serpentinization process and associated methane production occurring within the fault zone.

2 | THE LAPA GOLD DEPOSIT

In the Abitibi greenstone belt, antimony has been recognized along the major fault zones, particularly the CLLFZ and the Porcupine-Destor fault zones (Figure 1). The CLLFZ separates the Archaean Abitibi Subprovince from the Pontiac Subprovince to the south. In the Lapa area, schistosity is E–W oriented, dipping steeply to the north, parallel to bedding. A three-step evolution includes the thrusting of the greenstone belt onto the Pontiac Subprovince, a late extensional episode contemporaneous with the formation of the Timiskaming basins (2677–2673 Ma), followed by late dextral shearing with gold mineralization around 2665 Ma (Bedeaux, Pilote, Daigneault, & Rafini, 2017; Robert, 1989).

The main known antimony occurrence is the Lapa gold mine, located along a major flexure of the CLLFZ. Antimony is abundant in the upper part of the deposit, above a depth of 1100 m (Simard, Gaboury, Daigneault, & Mercier-Langevin, 2013). The main mineralized zone of the Lapa deposit is hosted in subvertical mafic and ultramafic rocks of Piché Group (2710 Ma, Pilote, Daigneault, David, & McNicoll, 2014), which are strongly deformed and altered, forming slivers within the CLLFZ (Simard et al., 2013) (Figure 2a). These rocks are in contact with the sedimentary Cadillac Group dated at 2687 Ma (Davis, 2002). Alteration is expressed as talc-rich serpentinized ultramafic rocks, strongly altered basalts (chlorite, carbonate, biotite/talc) and

remnants of amphibolite-rich mafic rocks. These associations are evidence of early CO₂ metasomatism (Schandl & Naldrett, 1992).

Two main ductile deformation events have been recognized; the first is characterized by an E-trending subvertical penetrative foliation, and was followed by the development of asymmetric Z-shaped folds that correspond to the late dextral shearing episode. A late brittle event is marked by quartz carbonate veins. Gold and antimony mineralization is predominantly hosted in highly strained and altered upper greenschist–lower amphibolite facies mafic to ultramafic rocks of the Piché Group. It consists of finely disseminated Au–Sb-enriched arsenopyrite–pyrrhotite ± pyrite, native gold disseminated in biotite- and carbonate-altered wall rocks, and Au–Sb quartz ± dolomite–calcite veinlets.

3 | SAMPLING AND METHODOLOGY

Ten rocks were sampled in the Lapa mine between depths of 510 and 890 m (Figure 2b). A mineralogical study on 20 polished sections was performed at the GeoRessources laboratory (Nancy, France) using a polarizing microscope (Olympus BX51). Accessory minerals were identified using a scanning electron microscope (HITACHI FEG S4800) coupled with an EDX spectrometer (Noran Vantage).

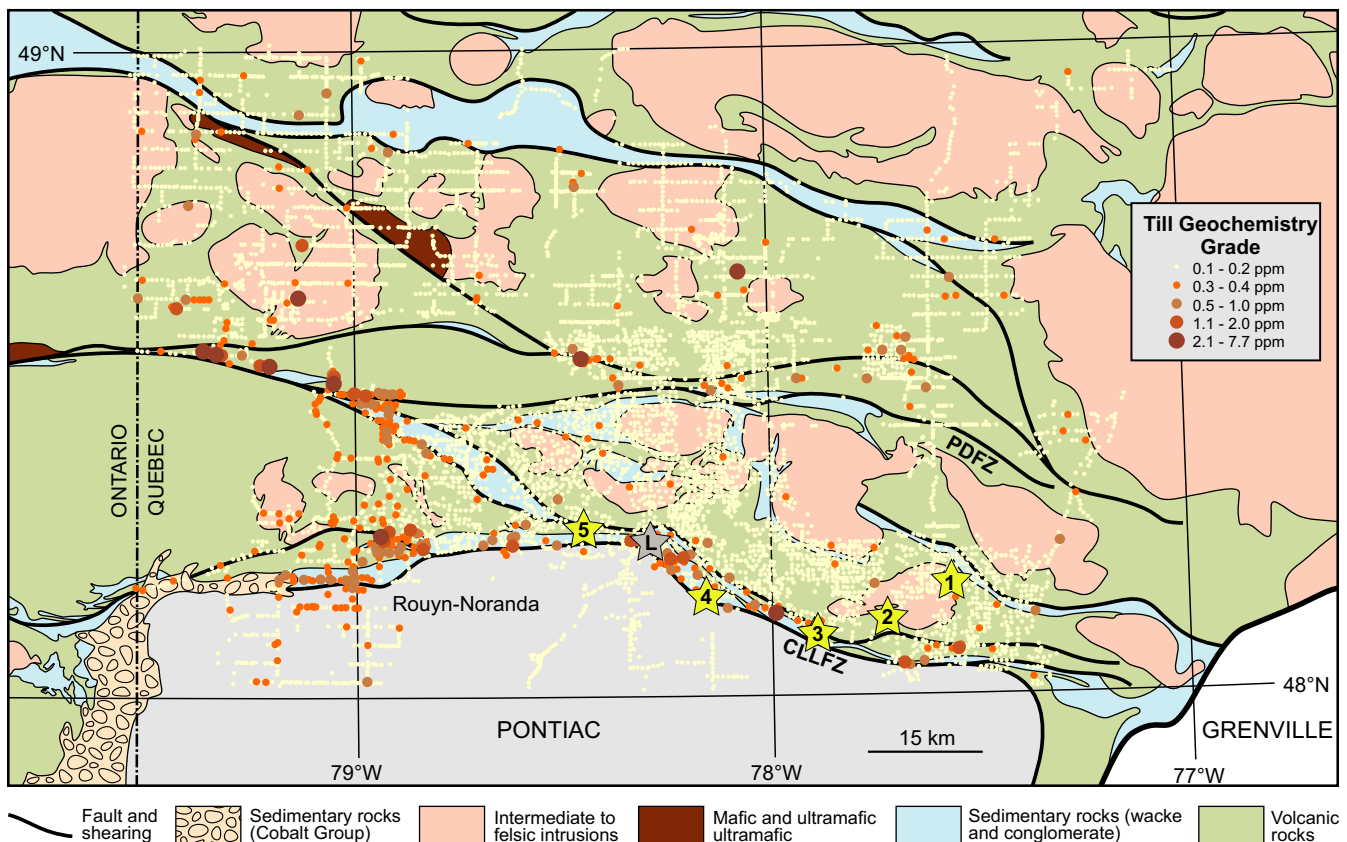


FIGURE 1 Geological map of the Eastern Abitibi greenstone belt, showing the distribution of antimony on till samples (data from Ministère des Ressources Naturelles, Québec), projet Cadillac, DP 87-22 [Colour figure can be viewed at wileyonlinelibrary.com]

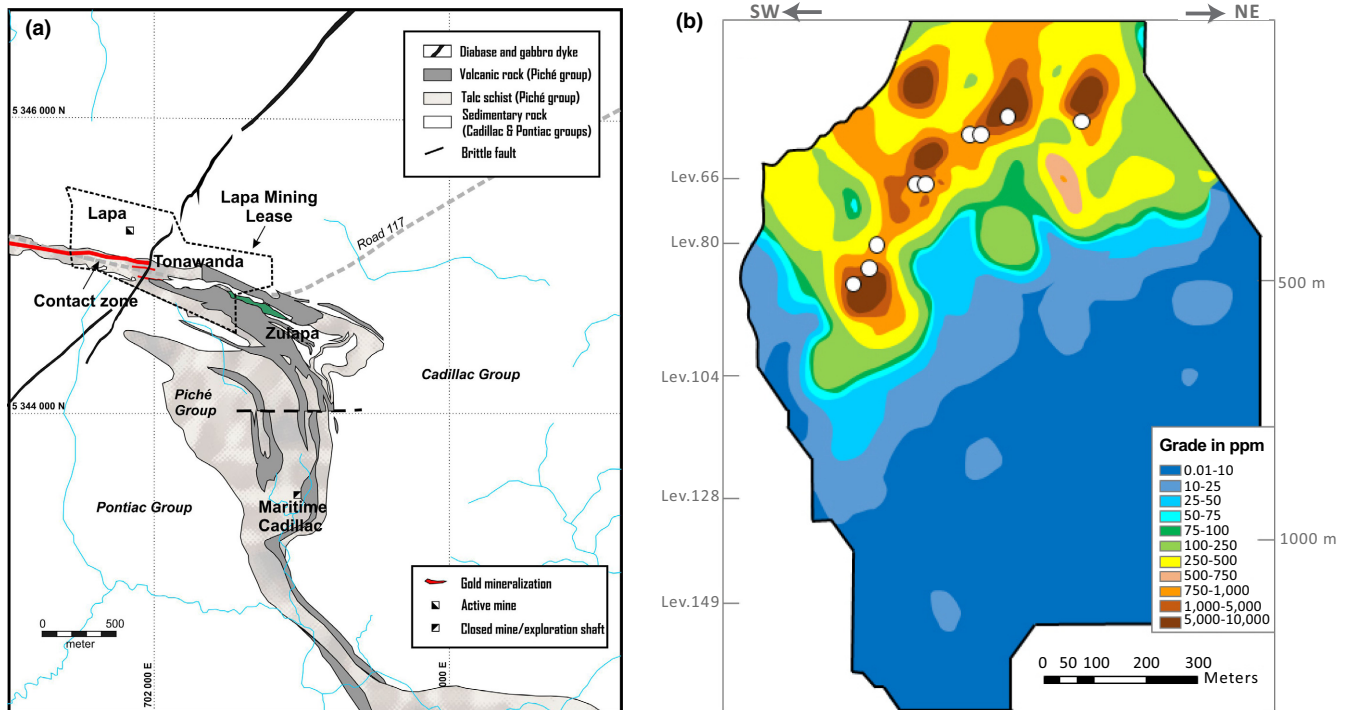


FIGURE 2 (a) Property geological map of the Lapa district; (b) Distribution of antimony along a longitudinal section of the Lapa mine, zone 1, and location of the samples [Colour figure can be viewed at wileyonlinelibrary.com]

Molar fractions of CO_2 , N_2 , CH_4 and H_2 were quantified in 57 fluid inclusions associated with the native antimony stage using *in situ* Raman spectra acquisitions performed using a LabRam HR microspectrometer ([®]Horiba Jobin Yvon) with an 800-mm focal distance, equipped with a $600 \text{ groove mm}^{-1}$ grating. The resulting spectral resolution at $\sim 1200 \text{ cm}^{-1}$ was 3.5 cm^{-1} . The 514.53-nm incident exciting radiation was delivered by an Ar-ion laser (Stabilite 2017, Spectra-Physics) with a power of 20 mW at the output of the objective (20x; N.A.:0.5 Olympus). The width of the spectrograph entrance slit was $100 \mu\text{m}$. An aperture of the confocal hole of $500 \mu\text{m}$ was chosen to optimize the signal/noise ratio. Specific attention was dedicated to the methane quantification following the analytical procedure described in Caumon et al. (2014).

4 | MINERALOGICAL EVOLUTION

The evolution of the deposit is characterized by five main steps (Figure 3):

1. A prograde greenschist facies assemblage of chlorite, albite and epidote, barren in gold, with an early stage of pyrrhotite, chalcocopyrite, pentlandite, chromite, ilmenite and titanite. Some tiny crystals of rounded ulmannite (NiSbS) are disseminated within the ultramafic talc schists (Figure 3a);
2. A prograde greenschist–lower amphibolite facies peak metamorphic assemblage characterized by Mg-hornblende and oligoclase in zones deeper than 1 km. The deposition of gold, in solid solution within finely disseminated arsenopyrite 1, occurs before the

peak of metamorphism (Simard et al., 2013). It is coeval with potassic alteration and pervasive silicification, and is followed by local mobilization of the invisible gold outside arsenopyrite 1 during the crystallization of arsenopyrite 2 associated with peak metamorphism. Early fine-grained disseminated arsenopyrite is rich in Co (up to 4647 ppm), Ni (up to 5562 ppm), Sb (up to 3298 ppm) and Au (1825 ppm) (Simard et al., 2013). These elements likely occur in solid solution and correlate with each other; ulmannite, berthierite and arsenopyrite are associated and aligned along the foliation (Figure 3b);

3. A low greenschist facies retrograde assemblage of actinolite–albite–chlorite;
4. A post-foliation fissural stage with quartz \pm dolomite–calcite veins, arsenopyrite, gold, antimony minerals, pyrrhotite, pyrite, chalcocopyrite and sphalerite (Figure 3c). Gold mineralization is mainly located in low-grade ultramafic rocks, as veins and veinlets in sulphide-rich volcanic and sedimentary rocks, in the fold noses of dextral asymmetric folds and in arsenopyrite-rich late quartz veins. Antimony minerals include berthierite (FeSb_2S_4), aurostibite (AuSb_2) and chalcostibite (CuSb_2S_2). Their matrix contains mainly quartz and a few crystals of calcite and biotite, locally with native gold on arsenopyrite. This process led to the dissolution of invisible gold from the arsenopyrite lattice and to the formation of native gold. The coexistence of stibnite and pyrite in equilibrium without gudmundite at the beginning of this stage indicates a temperature higher than 260°C (Williams-Jones & Normand, 1997);
5. A very late assemblage that includes berthierite, native antimony and stibnite as late infilling of veins (Figure 3d). No clear decomposition of aurostibite into native antimony + gold was observed,

implying that this late assemblage was precipitated directly from the fluid (Zheng et al., 2015).

5 | FLUID INCLUSION PETROGRAPHY AND COMPOSITION

The fluid inclusions are mainly pseudo-secondary and small, usually less than 10 μm (Figure 4). They express predominantly one phase (vapour or liquid) or two phases (liquid + vapour) at room temperature (Figure 4 and Table 1). Petrographic studies and Raman spectroscopic gas quantification allowed us to distinguish six types of fluid inclusion: one with only H_2O , and five others containing at least one of the following gases: N_2 , CH_4 , CO_2 , H_2 or CO . The salinities, estimated by Raman spectroscopy, range from 1.2 to 29.0 wt% eq. NaCl (Dubessy, Lhomme, Boiron, & Rull, 2002) in all the studied mine levels. Except for the highest level, 51, which shows a predominance of CO_2 , all the inclusions associated with native antimony are dominated by $\text{N}_2+\text{H}_2-\text{CH}_4$ (Figure 4). Some liquid-dominated inclusions have a certain amount of dissolved CH_4 , showing that not all the CH_4 was trapped within the vapour phase, indicating a high fluid pressure.

6 | DISCUSSION

The Lapa deposit belongs to a universal class of shear-zone-hosted mesothermal polymetallic Sb–(Au–W–Sn–As–Zn–Pb) deposits (Dill, 2010). It also shares strong similarities with the listvenite-type Au deposit, which is related to ultramafic magmatic rocks and

characterized by an assemblage of alteration minerals produced by carbon dioxide metasomatism of serpentinized ultramafic rocks. We will discuss the significance of this polyphase Au–Sb association and its possible relation with CH_4 fluids.

6.1 | Gold–antimony association

The following universal paragenetic stages have been recognized for Au–Sb deposits by Berger (1993) and Obolensky, Gushchina, Borisenko, Borovikov, and Nevol'ko (2009): (1) an early stage of mainly disseminated mineralization in wall rocks, characterized by pyrite, arsenopyrite and locally pyrrhotite, chalcopyrite, ferberite and scheelite; (2) a second stage marked by sulpho-antimonides; and (3) a final stage comprising stibnite, berthierite, gold and aurostibite.

These deposits may also display a rare fourth late paragenetic stage of native antimony, gudmundite, ulmannite, corynite (Ni(As,Sb)S) and gersdorffite, an association marked by nickel and antimony (Berger, 1993). This stage is seldom found coexisting with stibnite because their stability fields are separated by the field of berthierite (An & Zhu, 2010; Williams-Jones & Normand, 1997; Zheng et al., 2015). Native antimony is systematically associated with the presence of CH_4 (Fu, Mernagh, Fairmaid, Phillips, & Kendrick, 2014; Jaguin et al., 2013; Kontak, Horne, & Smith, 1996; Li et al., 2005; Normand, Gauthier, & Jébrak, 1996; Thorne, Lentz, Hoy, Fyffe, & Cabri, 2008; Yang, Lentz, Chi, & Kyser, 2004).

Depending on the temperature, $f\text{O}_2$ and total aqueous sulphur content, Sb is carried by either $\text{Sb}(\text{OH})_3$, $\text{Sb}_2\text{S}_2(\text{OH})_2$ or HSb_2S_4 in hydrothermal fluids. The solubility of Sb is reduced to less than 0.5% of the initial value by simple conductive cooling of a fluid from

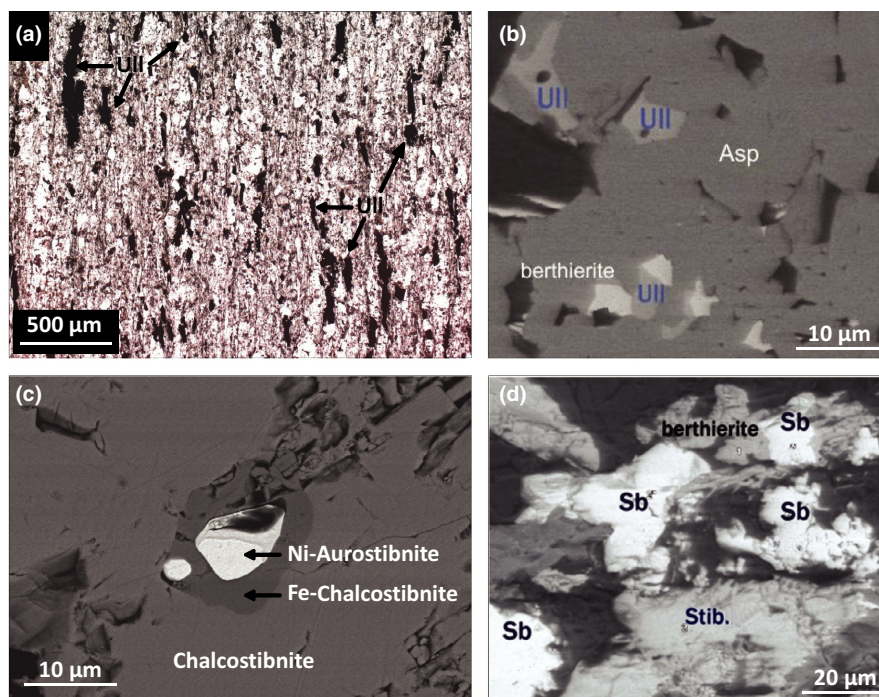


FIGURE 3 Microphotographs illustrating the paragenetic evolution of the Lapa antimony deposit. (a) Stage 1: prograde greenschist facies; (b) Stage 2: prograde greenschist–lower amphibolite facies; ulmannite (Ull) and arsenopyrite (Asp); (c) Stage 4: arsenopyrite, gold and antimony minerals; (d) Stage 5: berthierite, native antimony (Sb) and stibnite (Stib.) [Colour figure can be viewed at wileyonlinelibrary.com]

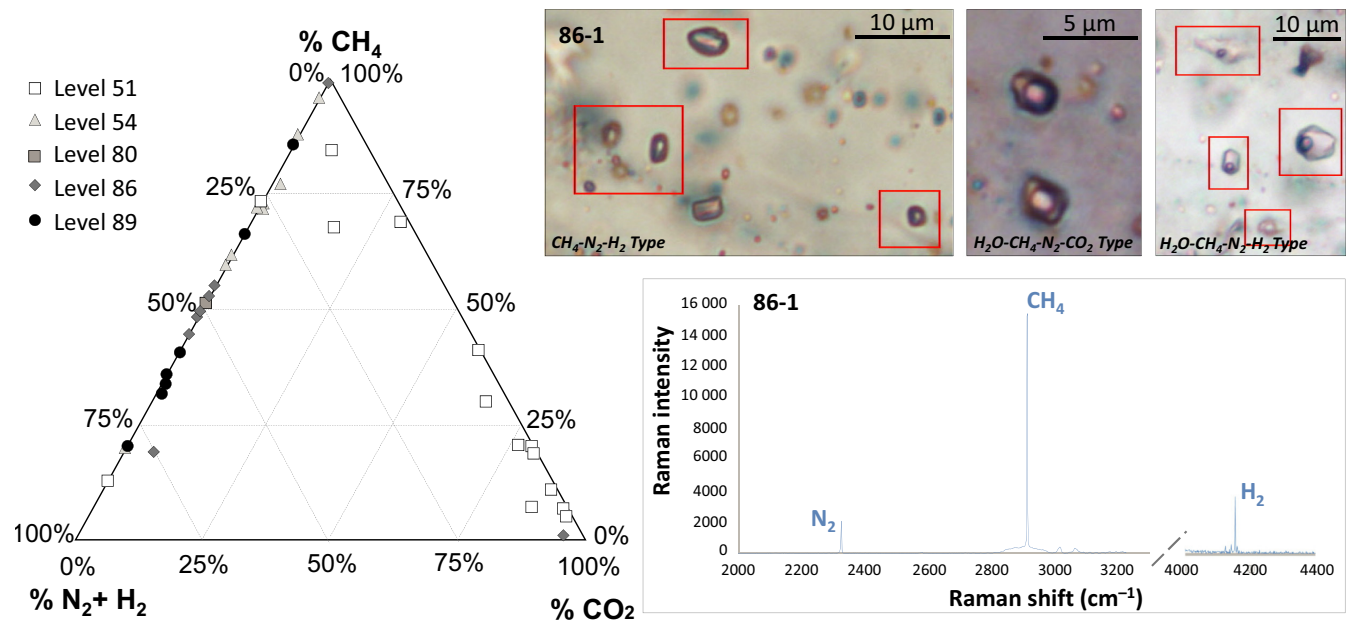


FIGURE 4 Petrographic characteristics and CO₂-CH₄-N₂+H₂ distribution in fluid inclusions from quartz of the Lapa mine [Colour figure can be viewed at wileyonlinelibrary.com]

TABLE 1 Characteristics of the fluid inclusions in quartz associated with the late antimony stage of the Lapa mine: microscopic observations and Raman results

Composition	H ₂ O	CH ₄ -N ₂ -H ₂	CH ₄ -CO ₂ -H ₂ -N ₂	H ₂ O-CH ₄ -N ₂ -CO ₂	H ₂ O-CH ₄ -H ₂ -N ₂	H ₂ O Graphite CH ₄ -N ₂ -CO ₂ -CO-H ₂
Number of fluid inclusions analysed	3	11	14	6	17	1
Shape	Elongated	Rounded or square	Rounded or square	Diamond or ovoid	Multiple	Square
Size	~5 μm	~3-4 μm	~3-4 μm	3-6 μm	2-10 μm	~8 μm
Habitus	Group	Group	Mostly group	Group and align along intra-mineral planes	Group and align along fault planes	Align with biphasic inclusion
Filling ratio (V/L)	0%	100%	100%	50%-80%	40%-60%	No value
%N ₂	0	47.39	15.96	4.10	38.72	33.42
%CH ₄	0	52.56	33.03	35.63	60.88	16.60
%H ₂	0	0.05	0.18	0	0.40	32.20
%CO ₂	0	0	50.89	60.27	0	5.21
%CO	0	0	0	0	0	12.58

350°C to 200°C (Krupp, 1988). Precipitation of native Sb would also occur by reduction due to low sulphur and oxygen fugacities (Krupp, 1988; Xie et al., 2017; Zheng et al., 2015; Zhu, Fang, & Tan, 2011). Two antimony parageneses may therefore be distinguished: an early one, which is oxidized and mainly associated with CO₂ and antimony sulphides, and a later one, which is more reduced, with CH₄ and native antimony. This two-stage Sb mineralization, from early gold to late antimony, has been interpreted either as a continuum (Nesbitt & Muehlenbachs, 1989; Xie et al., 2017), where mercury and antimony deposits were formed at relatively shallow depth (<3 km), or as the

superposition of a late epithermal system on early mesothermal gold mineralization, more than 100 Ma later (Bortnikov et al., 2010). The similar evolutions of the antimony parageneses in different deposits around the world calls for a continuum. In Lapa, the early enrichment of the sulphide phases in Sb and Ni, such as arsenopyrite (0.4% Sb; 1.5% Ni) and pyrite (4% Sb), suggests a continuity of Sb deposition, with a drastic change in the conditions of deposition, from oxidizing to reducing fluids; the high CH₄ content of the fluid inclusions related to the late native antimony stage is evidence of these reducing conditions.

6.2 | Origin of the methane

In the modern environment, deep saline ground waters within Precambrian continental shields may be rich in CH₄, locally at vast amounts exceeding 80% of the gas phase (Kietäväinen, Ahonen, Niinikoski, Nykänen, & Kukkonen 2017). Near the surface (<1.5 km), CH₄ is more likely produced at low temperatures from ancient organic compounds. Deeper, CH₄ has likely been formed by high-temperature abiotic synthesis, especially through reduction of CO₂ or CO by H₂ produced by serpentinization resulting from the reaction of water with ferrous-iron-rich minerals contained in ultramafic rocks (Schandl & Naldrett, 1992; Ethiopie & Schoell, 2014).

One of the key characteristics of antimony deposits is the abundance of methane (Kontak et al., 1996; Xie et al., 2017; Yang et al., 2004). CH₄ is also a minor but frequent component of fluids associated with orogenic gold mineralization (Gaboury, 2013 and references therein).

The early mineral associations in the Lapa deposits are typical of a CO₂-rich environment, and the high flux of H₂O–CO₂ was therefore preeminent, as in most orogenic gold deposits (Goldfarb & Groves, 2015). CO₂-rich carbonatation (listvenitization) occurs at high temperatures of around 290°–350°C (Ferenc, Uher, Spišiak, & Šimonova, 2016). Production of CH₄ has been described during serpentinization peaks between 200° and 315°C (McCollom & Bach, 2009) and therefore might become dominant only after the cessation of the CO₂ flux, at a lower temperature. Serpentinization is a long-term process that may have occurred continuously since the Archaean. It increased the weakness and decreased the overall permeability of fault zones, with the formation of non-connected domains that acted as semi-closed systems, allowing local concentrations of gas. Therefore, the age of the native antimony association could be much younger than that of the gold/antimony sulphide association. Pockets of methane have even been discovered in the present mine workings (Agnico-Eagle, personal communication).

The source of antimony remains unknown. The regional association of geochemical Sb anomalies (Figure 1), the Sb enrichments observed in gold deposits hosted by mafic rocks (Pitcairn et al., 2015) and the local Sb enrichment of lamprophyre in the Superior Province (Schandl & Gorton, 2000) suggests that more work is required to test the significance of this association.

7 | CONCLUSIONS

The antimony and gold association in the Lapa deposit reflects their common origin, derived from early polymetallic sulphides (ulmannite, arsenopyrite) in the ultramafic rocks of the Piché Group. The destabilization of these sulphides by early CO₂-rich fluids led to the formation of antimony sulphides and native gold in a more oxidizing environment. The conditions evolved to more reducing conditions, as reflected by the abundance of CH₄. Such methane could originate from the serpentinization of ultramafic rocks, and would allow the formation of native antimony in the upper part of the deposit.

The higher position of antimony does not reflect a true vertical zonation, but rather the superposition of CO₂-rich and CH₄-rich metallogenic environments. The time lag between these two events remains unknown, but the formation of native antimony could have occurred millions of years after native gold deposition.

ACKNOWLEDGEMENTS

The authors express their sincere appreciation to Agnico-Eagle Mines Ltd and the Lapa mine geology department staff for financial and logistical support, and for the authorization to publish. We acknowledge the Natural Sciences and Engineering Research Council of Canada for scholarships to MS and a Discovery grant to MJ. The GeoResources laboratory is thanked for providing mineralogical and Raman analyses. The authors are grateful to Marie-Camille Caumon (Raman Spectroscopy) and Sandrine Matthieu (SEM) for technical assistance during data acquisition. Comments on an early version of the paper by Dave Craw, Eva S. Schandl and an anonymous reviewer greatly helped to improve the paper. The authors do not have any conflict of interest.

ORCID

Michel Jébrak  <http://orcid.org/0000-0002-0473-9924>

REFERENCES

- Abrajano, T. A., Sturchio, N. C., Kennedy, B. M., Lyon, G. L., Muehlenbachs, K., & Bohlke, J. K. (1990). Geochemistry of reduced gas related to serpentinization of the Zambales ophiolites, Philippines. *Applied Geochemistry*, 5, 625–630.
- An, F., & Zhu, Y. (2010). Native antimony in the Baogutu gold deposit (west Junggar, NW China): Its occurrence and origin. *Ore Geology Reviews*, 37, 214–223.
- Ashley, P. M., & Craw, D. (2004). Structural controls on hydrothermal alteration and gold–antimony mineralisation in the Hillgrove area, NSW, Australia. *Mineralium Deposita*, 39, 223–239.
- Bedeaux, P., Pilote, P., Daigneault, R., & Rafini, S. (2017). Synthesis of the structural evolution and associated gold mineralization of the Cadillac Fault, Abitibi, Canada. *Ore Geology Reviews*, 82, 49–59.
- Bellot, J. P., Lerouge, C., Bailly, L., & Bouchot, V. (2003). The Biards Sb–Au-bearing zone (Massif Central, France): An indicator of crustal-scale transcurrent tectonics guiding late Variscan collapse. *Economic Geology*, 98, 1427–1447.
- Berger, V.I. (1993). *Descriptive, and grade and tonnage model for gold-antimony deposits*. USGS, open file report 93-194 (pp. 27). U.S. Geological Survey, Reston, Virginia, United States.
- Bigot, L., & Jébrak, M. (2015). Gold mineralization at the Syenite-hosted Beattie Gold Deposit, Duparquet, Neoproterozoic Abitibi Belt, Canada. *Economic Geology*, 110, 315–335.
- Bortnikov, N.S., Gamunin, G.N., Vilent'eva, O.V., Prokof'ev, V.Yu., & Prokof'ev, A.V. (2010). The Sarylakh and Sentachan Gold-antimony Deposits, Sakha-Yakutia: A case of combined mesothermal gold-quartz and epithermal stibnite ores. *Geology of Ore Deposits*, 52, 339–372.
- Boyle, G.O. (1990). Hillgrove antimony-gold deposits. In *Geology of the mineral deposits of Australia and Papua New Guinea*. F. E. Hughes, ed. Australasian Institute of Mining and Metallurgy, 14, 1425–1427.

- Caumon, M. C., Robert, P., Laverret, E., Tarantola, A., Randi, A., Pironon, J., ... Girard, J. P. (2014). Determination of methane content in NaCl-H₂O fluid inclusions by Raman spectroscopy. Calibration and application to the external part of the Central Alps (Switzerland). *Chemical Geology*, 378–379, 52–61.
- Chauris, L., & Marcoux, É. (1994). Metallogeny of the Armorican Massif. In: *Pre-Mesozoic geology France and related areas* (J.D. Keppie, ed.) part II. C Metallogeny, Springer Verlag, 243–264.
- Colvine, A. C. (1989). An empirical model for the formation of Archean gold deposits: Products of final cratonization of the Superior Province, Canada. *Economic Geology Monograph*, 6, 37–53.
- Cooke, D. R., & Simmons, S. F. (2000). Characteristics and genesis of epithermal gold deposits. *Society of Economic Geologists Reviews*, 13, 221–244.
- Czarnota, K., Blewett, R. S., & Goscombe, B. (2010). Predictive mineral discovery in the eastern Yilgarn Craton, Western Australia: An example of district scale targeting of an orogenic gold mineral system. *Precambrian Research*, 183, 356–377.
- Davis, D. W. (2002). U-Pb geochronology of Archean metasedimentary rocks in the Pontiac and Abitibi subprovinces, Quebec, constraints on timing, provenance and regional tectonics. *Precambrian Research*, 115, 97–117.
- Davis, D. R., Paterson, D. B., & Griffiths, D. H. C. (1986). Antimony in South Africa. *Journal of The South African Institute of Mining and Metallurgy*, 86, 173–193.
- Debret, B., Andreani, M., Godard, M., Nicollet, C., Schwartz, S., & Lafay, R. (2013). Trace element behaviour during serpentinization/de-serpentinization of an eclogitized oceanic lithosphere: A LA-ICPMS study of the Lanzo ultramafic massif (Western Alps). *Chemical Geology*, 357, 117–133.
- Deschamps, F., Guillot, S., Godard, M., Andreani, M., & Hattori, K. (2011). Serpentinites act as sponges for fluid-mobile-elements in abyssal and subduction zone environments. *Terra Nova*, 23, 171–178.
- Dill, H. G. (2010). The "chessboard" classification scheme of mineral deposits: Mineralogy and geology from aluminium to zirconium. *Earth-Science Reviews*, 100, 1–420.
- Dubé, B., & Gosselin, P. (2007). Greenstone-hosted quartz-carbonate vein deposits. In W. D. Goodfellow, ed., *Mineral Deposits of Canada: A Synthesis of Major Deposit-Types, District Metallogeny, the Evolution of Geological Provinces & Exploration Methods: Geological Association of Canada, Mineral Deposits Division, Special Publication No. 5*, p. 49–73.
- Dubessy, J., Lhomme, T., Boiron, M.-C., & Rull, F. (2002). Determination of chlorinity in aqueous fluids using Raman spectroscopy of the stretching band of water at room temperature: Application to fluid inclusions. *Applied Spectroscopy*, 56, 99–106.
- Ethiopia, G., & Schoell, M. (2014). Abiotic gas: Atypical, but not rare. *Elements*, 10, 291–296.
- European Commission, 2011. Tackling the Challenges in Commodity Markets and Raw Materials. COM (2011) 25 final, Brussels.
- Ferenc, S., Uher, P., Spišiak, J., & Simonova, V. (2016). Chromium- and nickel-rich micas and associated minerals in listvenite from the Muránska Zdyčava, Slovakia: Products of hydrothermal metasomatic transformation of ultrabasic rock. *Journal of Geosciences*, 61, 239–254.
- Fu, B., Mernagh, T. P., Fairmaid, A. M., Phillips, D., & Kendrick, M. A. (2014). CH₄-N₂ in the Maldon gold deposit, central Victoria, Australia. *Ore Geology Reviews*, 58, 225–237.
- Gaboury, D. (2013). Does gold in orogenic deposits come from pyrite in deeply buried carbon-rich sediments? Insight from volatiles in fluid inclusions. *Geology*, 41, 1207–2011.
- Goldfarb, R.J., Baker, T., Dubé, B., Groves, D.I., Hart, C.J.R., & Gosselin, P. (2005). Distribution, character, and genesis of gold deposits in metamorphic terranes. *Economic Geology 100th Anniversary*, 100: 407–450.
- Goldfarb, R. J., & Groves, D. I. (2015). Orogenic gold: Common or evolving fluid and metal sources through time. *Lithos*, 233, 2–26.
- Goldfarb, R. J., Groves, D. I., & Gardoll, S. (2001). Orogenic gold and geologic time: A global synthesis. *Ore Geology Reviews*, 18, 1–75.
- Groves, D. I., Goldfarb, R. J., Gebre-Mariam, M., Hagemann, S. G., & Robert, F. (1998). Orogenic gold deposits: A proposed classification in the context of their crustal distribution and relationship to other gold deposit types. *Ore Geology Reviews*, 13, 7–27.
- Hagemann, S. G., & Lüders, V. (2003). P-T-X Conditions of Hydrothermal Fluids and Precipitation Mechanism of Stibnite gold Mineralization at the Wiluna Lode-gold Deposits, Western Australia: Conventional and Infrared Microthermometric Constraints. *Mineralium Deposita*, 38, 936–952.
- Jaguin, J., Boulvais, P., Poujol, M., Bosse, V., Paquette, J. L., & Vilbert, D. (2013). Albitization in the Antimony Line, Murchison Greenstone Belt (Kaaopvaal Craton): A geochemical and geochronological investigation. *Lithos*, 168–169, 124–143.
- Kerrick, R. (1986). Fluid transport in lineaments. *Philosophical Transactions of the Royal Society of London*, 317, 219–251.
- Kerrick, R., & Ludden, J. (2000). The role of fluids during formation and evolution of the southern Superior Province lithosphere: An overview. *Canadian Journal of Earth Sciences*, 37, 135–164.
- Kietäväinen, R., Ahonen, L., Niinikoski, P., Nykänen, H., & Kukkonen, I. T. (2017). Abiotic and biotic controls on methane formation down to 2.5 km depth within the Precambrian Fennoscandian Shield. *Geochimica Cosmochimica Acta*, 202, 124–145.
- Kontak, D. J., Horne, R. J., & Smith, P. K. (1996). Hydrothermal characterization of the West Gore Sb-Au deposit, Meguma Terrane, Nova Scotia, Canada. *Economic Geology*, 91, 1239–1262.
- Krupp, R. E. (1988). Solubility of stibnite in hydrogen sulfide solutions, speciation, and equilibrium constants, from 25 to 350°C. *Geochimica et Cosmochimica Acta*, 52, 3005–3015.
- Lehrberger, G. (1992). Metallogenese von Antimonit-Gold-Lagerstätten in marinen Sedimenten der Ostkordillere Boliviens. *Münchner Geologische Hefte*, 6, 204.
- Li, C. Y., Liu, Y. P., Zhang, Q., Pi, D. H., Zhang, W. L., & Chen, J. (2005). Discovery of antimony and distribution characteristics of associated elements in Huize Pb-Zn deposit. *Mineral Deposits*, 24, 52–60. (in Chinese with English abstract).
- McCollom, T. M., & Bach, W. (2009). Thermodynamic constraints on hydrogen generation during serpentinization of ultramafic rocks. *Geochimica Cosmochimica Acta*, 73, 856–875.
- Nesbitt, B. E., & Muehlenbachs, K. (1989). Geology, geochemistry and genesis of mesothermal lode gold deposits of the Canadian Cordillera. Evidence for ore formation from evolved meteoritic waters. *Economic Geology Monograph*, 6, 553–563.
- Normand, C., Gauthier, M., & Jébrak, M. (1996). The Québec antimony deposit: An example of gudmundite- native antimony mineralization in the ophiolitic mélange of the southeastern Quebec Appalachians. *Economic Geology*, 91, 149–163.
- Obolensky, A. A., Gushchina, L. V., Borisenko, A. S., Borovikov, A. A., & Nevol'ko, P. A. (2009). Computer thermodynamic modeling of the transport and deposition of Sb and Au during the formation of Au-Sb deposits. *Russian Geology and Geophysics*, 50, 950–965.
- Pearson, T.N., & Viljoen, M.J. (1986). *Antimony Mineralization in the Murchison Greenstone Belt - An Overview*. In: Mineral Deposits of Southern Africa (C.R. Anhaeusser & S. Maske, eds), The Geological Society of South Africa, Johannesburg. 293–320.
- Phillips, G. N., & Evans, K. A. (2004). Role of CO₂ in the formation of gold deposits. *Nature*, 429, 860–863.
- Pilote, P., Daigneault, R., David, J., & McNicoll, V. (2014). Architecture of the Malartic, Piché and Cadillac groups and the Cadillac Fault, Abitibi. Geological revision, new dates and interpretations. Session 12, Québec Mine, DV 2014-08, p. 75, MERN.
- Pitcairn, I. K., Craw, D., & Teagle, D. A. H. (2015). Metabasalts as sources of metals in orogenic gold deposits. *Mineralium Deposita*, 50, 373–390.

- Pochon, A., Gapais, D., Gloaguen, E., Gumiaux, Ch, Branquet, Y., Cagnard, F., & Martelet, G. (2016). Antimony deposits in the Variscan Armorican belt, a link with mafic intrusives. *Terra Nova*, 28, 138–145.
- Robert, F. (1989). The internal structure of the Cadillac tectonic zone southeast of Val d'Or, Abitibi belt, Québec. *Canadian Journal of Earth Sciences*, 26, 2661–2675.
- Schandl, E. S., & Gorton, M. P. (2000). Sb-enriched ultramafic lamprophyre in the Hemlo Au-Mo deposit of the Superior Province, Canada: Evidence for Post-Archean Sb mobility. *European Journal of Mineralogy*, 12, 625–637.
- Schandl, E. S., & Naldrett, A. J. (1992). CO₂ metasomatism of serpentinites, south of Timmins, Ontario. *Canadian Mineralogist*, 30, 93–108.
- Simard, M., Gaboury, D., Daigneault, R., & Mercier-Langevin, P. (2013). Multistage gold mineralization at the Lapa mine, Abitibi Subprovince: Insights into auriferous hydrothermal and metasomatic processes in the Cadillac - Larder Lake Fault Zone. *Mineralium Deposita*, 48, 883–905.
- Thorne, K. G., Lentz, D. R., Hoy, D., Fyffe, L. R., & Cabri, L. J. (2008). Characteristics of mineralization at the main zone of the Clarence Stream gold deposit, southwestern New Brunswick, Canada: Evidence for an intrusion-related gold system in the Northern Appalachian Orogen. *Exploration and Mining Geology*, 17, 13–49.
- Tomkins, A. G., Pattison, D. R. M., & Zaleski, W. (2004). The Hemlo Gold deposit, Ontario: An example of melting and mobilization of precious metal-sulfosalt assemblage during amphibolite facies metamorphism and deformation. *Economic Geology*, 99, 1063–1084.
- White, N.C., & Hedenquist, J.W. (1990). *Epithermal environments and styles of mineralization: Variations and their causes, and guidelines for exploration*. In: *Epithermal Gold Mineralization of the Circum-Pacific: Geology, Geochemistry, Origin and Exploration* (J. Hedenquist, N. C White, G. Siddeley & G., eds). *Journal of Geochemical Exploration*, 36, 445–474.
- Williams-Jones, A. E., & Normand, C. (1997). Controls of mineral parageneses in the system Fe–Sb–S–O. *Economic Geology*, 92, 308–324.
- Xie, Z.-J., Xin, Y., Cline, J. S., Yan, B.-W., Wang, Z.-P., Tan, Q. P., & Wei, D.-T. (2017). Comparison of the native antimony-bearing Paiting gold deposit, Guizhou Province, China, with Carlin-type gold deposits, Nevada, USA. *Mineralium Deposita*, 52, 69–84.
- Yang, X. M., Lentz, D. R., Chi, G., & Kyser, T. K. (2004). Fluid-mineral reaction in the Lake George granodiorite, New Brunswick, Canada: Implications for Au-W-Mo-Sb mineralization. *Canadian Mineralogist*, 42, 1443–1464.
- Zhai, W., Sun, X., Yi, J., Zhang, X., Mo, R., Zhou, F., . . . Zeng, Q. (2014). Geology, geochemistry, and genesis of gold-antimony mineralization in the Himalayan Orogen, South Tibet, China. *Ore Geology Reviews*, 58, 68–90.
- Zheng, B., Zhu, Y., An, F., Huang, Q.-Y., & Qiu, T. (2015). As-Sb-Bi-Au mineralization in the Baogutu gold deposits, Xinjiang, NW China. *Ore Geology Reviews*, 69, 17–32.
- Zhu, Y., Fang, A., & Tan, J. (2011). Geochemistry of hydrothermal gold deposits: A review. *Geoscience Frontiers*, 2, 367–374.

How to cite this article: Jébrak M, Lebrun C, André-Mayer A-S, Simard M. Native antimony emplaced by methane-rich hydrothermal fluid in an orogenic fault-zone. *Terra Nova*. 2017;29:401–408. <https://doi.org/10.1111/ter.12300>